Molecular Therapy
Oncolytics
Original Article

Perturbing DDR signaling enhances cytotoxic effects of local oncolytic virotherapy and modulates the immune environment in glioma

Marilin S. Koch,[1] Mykola Zdioruk,[1] Michal O. Nowicki,[1] Alec M. Griffith,[2] Estuardo Aguilar-Cordova,[3] Laura K. Aguilar,[3] Brian W. Guzik,[3] Francesca Barone,[3] Paul Peter Tak,[3] Katharina Schregel,[4] Michael S. Hoetker,[5] James A. Lederer,[2] E. Antonio Chiocca,[1] Ghazaleh Tabatabai,[6] and Sean E. Lawler[1,7]

[1]Harvey Cushing Neurooncology Research Laboratories, Department of Neurosurgery, Brigham and Women's Hospital, Harvard Medical School, 60 Fenwood Road, Boston, MA 02115, USA; [2]Department of Surgery, Brigham & Women's Hospital, Harvard Medical School, 75 Francis Street, Boston, MA 02115, USA; [3]Candel Therapeutics, 117 Kendrick St, Suite 450, Needham, MA 02494, USA; [4]Department of Neuroradiology, University Hospital Heidelberg, Im Neuenheimer Feld 400, 69120 Heidelberg, Germany; [5]Department of Molecular Biology, Massachusetts General Hospital, 185 Cambridge St, Boston, MA 02114, USA; [6]Department of Neurology and Interdisciplinary Neuro-Oncology, University Hospital Tübingen, Hertie Institut for Clinical Brain Research, Eberhard Karls University Tübingen, Hoppe-Seyler-Straße 6, 72076 Tübingen, Germany

CAN-2409 is a replication-deficient adenovirus encoding herpes simplex virus (HSV) thymidine kinase (tk) currently in clinical trials for treatment of glioblastoma. The expression of tk in transduced cancer cells results in conversion of the pro-drug ganciclovir into a toxic metabolite causing DNA damage, inducing immunogenic cell death and immune activation. We hypothesize that CAN-2409 combined with DNA-damage-response inhibitors could amplify tumor cell death, resulting in an improved response. We investigated the effects of ATR inhibitor AZD6738 in combination with CAN-2409 *in vitro* using cytotoxicity, cytokine, and fluorescence-activated cell sorting (FACS) assays in glioma cell lines and *in vivo* with an orthotopic syngeneic murine glioma model. Tumor immune infiltrates were analyzed by cytometry by time of flight (CyTOF). *In vitro*, we observed a significant increase in the DNA-damage marker γH2AX and decreased expression of PD-L1, pro-tumorigenic cytokines (interleukin-1β [IL-1β], IL-4), and ligand NKG2D after combination treatment compared with monotherapy or control. *In vivo*, long-term survival was increased after combination treatment (66.7%) compared with CAN-2409 (50%) and control. In a tumor re-challenge, long-term immunity after combination treatment was not improved. Our results suggest that ATR inhibition could amplify CAN-2409's efficacy in glioblastoma through increased DNA damage while having complex immunological ramifications, warranting further studies to determine the ideal conditions for maximized therapeutic benefit.

INTRODUCTION

Glioblastoma (GBM) is the most common malignant primary brain tumor,[1] with a median overall survival of only 14.6 months under aggressive multimodal treatment including surgery and radiochemotherapy.[2] Features contributing to therapeutic resistance in GBM include infiltrative proliferation and neovascularization, extensive tumor heterogeneity, a low mutational load, and an immunosuppressive microenvironment.[3–6] Attempts to overcome these obstacles include the use of drugs targeting angiogenesis[6–9] and EGFR mutations.[10,11] Alternating electric fields,[12] checkpoint inhibitors,[13] neoantigen vaccines,[14] and oncolytic viruses[15] have been also used. Despite encouraging results, none of these strategies have proved to be successful as single agents, suggesting the need of combination therapies.

CAN-2409 is a suicide-gene system consisting of the herpes simplex virus thymidine kinase (HSV-tk)-expressing adenovirus CAN-2409 and the pro-drug ganciclovir (GCV). GCV is phosphorylated by HSV-tk and cellular kinases to GCV triphosphate, which acts as a nucleoside analog of dGTP. Incorporation of nucleoside analogs into the actively replicating cells interferes with DNA synthesis and leads to accumulation of DNA damage, ultimately causing apoptotic and necrotic cell death.[16–22] This effect is delivered in combination with the immunogenic activity of the adenovirus backbone, which induces stimulation of the innate and acquired immune system, resulting in upregulation of inflammatory cytokines, co-stimulatory molecules, and recruitment/activation of anti-tumor effector cells.[23,24]

In a phase 1 b/2a clinical trial, CAN-2409 treatment in addition to standard of care (SoC) therapy has been shown to significantly

Received 2 March 2022; accepted 22 July 2022;
https://doi.org/10.1016/j.omto.2022.07.009.

[7]Present address: Department of Pathology and Laboratory Medicine, Legorreta Cancer Center, Brown University, 70 Ship Street, Providence, RI 02903, USA

Correspondence: Sean E. Lawler, PhD, Associate Professor, Harvey Cushing Neurooncology Research Laboratories, Department of Neurosurgery, Brigham and Women's Hospital, Harvard Medical School, 60 Fenwood Road, Boston, MA 02115, USA.
E-mail: sean_lawler@brown.edu

prolong overall survival of patients with GBM compared with SoC alone (CAN-2409 plus SoC 17.1 months versus SoC 13.5 months).[25] In this setting, the combination of CAN-2409 with anti-PD-1 led to increased intratumoral T cell infiltration and a higher percentage of long-term-surviving animals[26] and is currently under investigation in a phase 1 clinical trial ("Phase I Study of Neoadjuvant CAN-2409 Plus Immune Checkpoint Inhibitor Combined With Standard of Care for Newly Diagnosed High-Grade Gliomas," ClinicalTrials.gov: NCT03576612).

DNA-damage response (DDR) signaling is triggered upon occurrence of DNA damage. Central upstream regulators of this pathway are the serine-threonine kinases ataxia telangiectasia mutated (ATM) and ataxia telangiectasia and Rad3-related (ATR). ATM and ATR are activated by the presence of double-strand beaks and replication stress and lead to the phosphorylation of the downstream targets CHK1 and CHK2. This results in cell-cycle arrest and enables the repair of DNA lesions before the cells enter mitosis, thus preventing apoptosis. ATR and ATM inhibitors have been shown to cross the blood-brain barrier[27–29] and are currently under investigation in several clinical trials as treatment options for numerous cancer entities.

As the mode of action of CAN-2409 is mediated by the induction of DNA damage, we hypothesized that a disruption of DDR signaling may significantly improve its therapeutic efficacy. In this study, we investigated the effects of ATR (and ATM) inhibition on the cytotoxic and immunogenic components of CAN-2409 both *in vitro* and *in vivo* to determine the significance of this pathway in local gene-suicide immunotherapies. Our data demonstrated that CAN-2409 induces a DDR response in GBM cells and that co-treatment with the ATR inhibitor AZD6738 and CAN-2409 leads to synergistic increases in tumor cell death *in vitro* and improved *in vivo* survival. Our data suggest that combination of CAN-2409 with DDR inhibition should be explored in humans. Further studies are needed to fully understand the effects of this combination on anti-tumor immunity.

RESULTS

CAN-2409-induced DNA damage is significantly enhanced by ATR/ATM inhibition

The ability of CAN-2409 to cause DNA damage has been previously demonstrated.[26] We hypothesized that inhibition of DNA repair would enhance its tumor-killing effects. To assess this, we measured the levels of γH2AX, a phosphorylated form of H2AX, indicative of double-stranded DNA breaks, in the presence of small-molecule selective inhibitors of either the ATM or ATR kinases. CAN-2409 was administered as monotherapy and in combination therapy with the ATR inhibitor AZD6738 or the ATM inhibitor AZD1390. Combination treatment of CAN-2409 with AZD6738 resulted in significantly higher γH2AX levels compared wiht both monotherapies and untreated control in both the glioma stem cell (GSC)-like line G9-pCDH (Figure 1A) and an established cell line, U1242 MG (Figure 1B). For the combination with ATM-inhibitor AZD1390, we observed the same dynamics in the GSC lines (Figures S1A and S1B), while this was not the case for U1242 MG cells, where additional treatment with AZD1390 led to a decrease of γH2AX (Figures S1C and S1D).

Combination of CAN-2409 and ATR inhibition acts synergistically in tumor cell killing

Enhanced γH2AX levels after combinatorial treatment with CAN-2409 and AZD6738 or AZD1390 indicate the potential for increased tumor cell killing via reinforced and unresolved DNA damage. To further explore this hypothesis, we performed cell viability assays with CAN-2409 in combination with AZD6738 or AZD1390. Combining both CAN-2409 and AZD6738 led to synergistic tumor cell death in the GSCs and the U1242 MG cells (Figures 1C and 1D) by far exceeding the cytotoxic effect of the monotherapies. This was not the case for the cells treated with the ATM-inhibitor AZD1390, where the overall therapeutic effect was far less pronounced, and synergistic activity did not reliably occur across cell lines (Figures S1C and 1D) for unknown reasons. Considering the superior and consistent results after ATR inhibition, we further continued our study with the ATR-inhibitor AZD6738. The effect of the ATR-inhibitor AZD6738 on its downstream target CHK1 was validated by immunoblots that demonstrated a diminished abundance of total and phosphorylated CHK1 after treatment (Figures 1E and 1F); total CHK1 is probably reduced due to degradation upon genotoxic stress as demonstrated previously.[30] The untreated U1242_LRP cell line, in contrast to G9_pCDH, already has a high expression of pCHK1, suggesting elevated basal activation of the DDR signaling pathway that might account for the differences seen in the cell lines as outlined above.

Enhancement of efficacy in mouse GBM models by the combination of CAN-2409 and ATR inhibition

To explore a potential enhancement of CAN-2409 efficacy by addition of the DNA-damage-repair inhibitor AZD6738 *in vivo*, we performed a survival study utilizing the immunocompetent syngeneic GL261 GBM model (Figure 2A). Treatment was started 7 days after tumor implantation. In the analysis, no difference in median survival was observed between the control (28.5 days) and the AZD6738 monotherapy group (29 days); in contrast, both CAN-2409 and combination treatment resulted in long-term survival (>125 days) in 50%–66% of the animals. Combination treatment proved to significantly prolong survival (control versus combination $p = 0.0022$) (Figure 2B). Compared with CAN-2409 alone, the combination therapy was more effective: 50% (3/6) of the CAN-2409-treated animals reached endpoint until day 29, leading to a median survival of 77 days. 66.7% (4/6) of the animals that were treated with CAN-2409+AZD6738 were alive when the experiment was terminated and the curves right censored (day 125 after tumor cell implantation). Since the survival of >50% of the combination-treated animals exceeded the experiment termination date, no median survival for this group can be stated. These results were supported by our imaging results: the magnetic resonance imaging (MRI) analysis of all groups in the survival experiment revealed

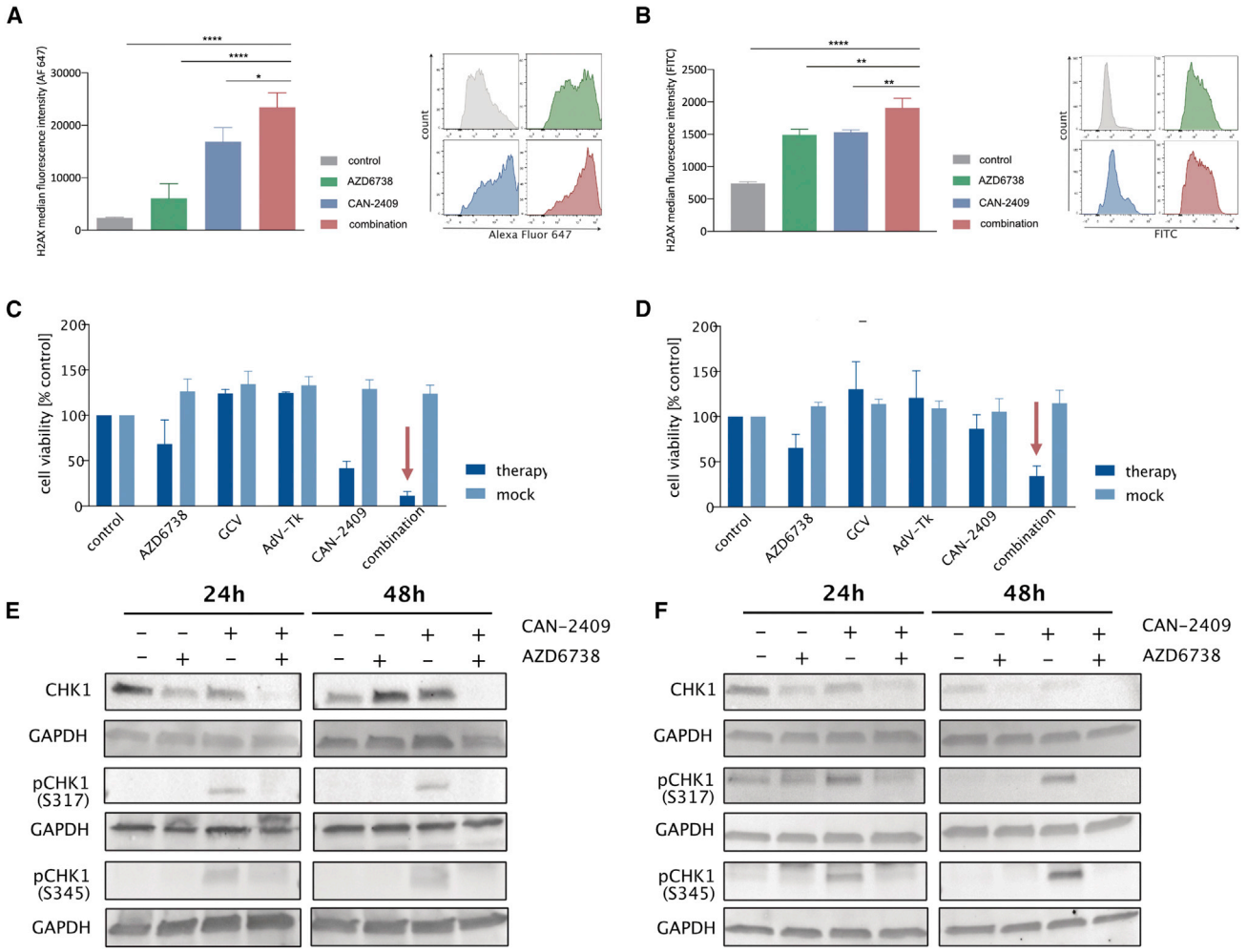

Figure 1. Increased DNA damage mediates enhanced cytotoxic tumor cell killing after combined treatment with ATRi and CAN-2409

(A and B) B H2AX FACS for the combination of CAN-2409 and ATR inhibitor AZD6738 in G9_pCDH (A) and U1242_LRP (B). H2AX is a surrogate parameter for double-strand breaks and is significantly enhanced in the combined treatment with CAN-2409 and ATRi compared with control ($p < 0.0001$ for G9_pCDH and $p < 0.0001$ for U1242_LRP), AZD6738 ($p < 0.0001$ for G9_pCDH and $p = 0.0002–0.001$ for U1242_LRP), and CAN-2409 ($p = 0.0243–0.042$ for G9_pCDH and $p < 0.0001–p = 0.002$ for U1242_LRP), biological replicates = 2, technical replicates = 3. (C and D) Cell viability assays for the combination of CAN-2409 and ATR inhibitor AZD6738 in G9_pCDH (C) and U1242_LRP (D) showing synergistic tumor cell killing in the combination treatment compared with CAN-2409 and AZD6738 monotherapy. Synergy calculation was performed with the Chou-Talalay method.[31] (E and F) Immunoblots after treatment with CAN-2409 and/or AZD6738. Immunoblots showing protein expression of ATR downstream target CHK1. AZD6738 attenuates CAN-2409-induced pCHK1 in G9_pCDH (E) and U1242_LRP (F). Total CHK1 is also reduced, possibly due to degradation upon genotoxic stress.[40]

significant progressive tumor growth in both control (3/3) and AZD6738 (3/3) and slight tumor progression in CAN-2409-treated (3/3) animals. In contrast, the combination treatment cohort presented without tumorous lesions in 2/3 imaged animals (Figure 2C).

Long-term-surviving animals were re-challenged with a second GL261fluc tumor cell implantation into the contralateral hemisphere without any subsequent therapy with 16- to 18-week-old age-matched tumor-naïve mice used as controls. While animals treated previously with CAN-2409 alone exhibited a significantly prolonged survival compared with untreated controls, we did not observe the same for combination-treated animals (Figure S2). Animals that underwent therapy with both CAN-2409 and AZD6738 showed a longer median survival (56 days) compared with control (31 days), but this was not statistically significant.

DDR disruption modifies the CAN-2409-induced cytokine profile

Despite gliomas being considered immunologically "cold" tumors, cytokines play a key role in GBM development and maintenance and can be classified into pro- and anti-tumorigenic (Figure 3A). CAN-2409 has been shown to not only initiate tumor cell death but also induce a T helper type 1 (Th1)-like cytokine profile,[23] thereby

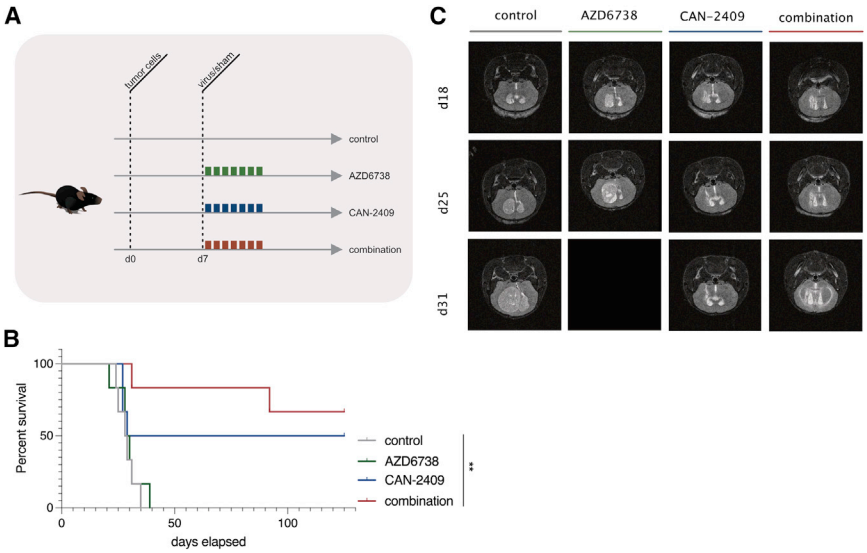

Figure 2. Treatment with CAN-2409 under concomitant blockade of the ATR-CHK1 pathway leads to improved survival *in vivo*

(A) Experimental setup for *in vivo* survival study. 100,000 GL261fluc cells were injected stereotactically into the right hemisphere. 7 days later, CAN-2409/sham was injected into the same location, followed by treatment with ganciclovir and/or AZD6738 for a total of 7 days. Endpoint was considered as a weight loss of 20%, onset of neurological symptoms, or signs of pain and distress. n = 6 per group. (B) Kaplan-Meier survival curves. No difference in median survival between untreated control (28.5 days) and AZD6738 monotherapy (29 days) were observed, while CAN-2409 treatment resulted in a prolonged median survival (77 days) that was enhanced by AZD6738. More than 50% of the animals that received combinatorial treatment survived beyond the experiment termination date (125 days). Combined treatment with CAN-2409 and AZD6738 significantly prolonged survival (control versus combination p = 0.0022). Log rank test was used to determine significance. (C) Prospective MRI analysis of tumor formation of *in vivo* survival study. 3 animals per group of the survival study underwent MR imaging 18, 25, and 31 days after tumor implantation. Massive progressive tumor growth was noted in all animals of the control and AZD6738-treatment cohort. Only slight tumor progression was observed in the CAN-2409 group, while the combination cohort presented possible tumor growth in one animal only.

contributing to an anti-tumor immune response. We therefore investigated the effects of a concomitant ATR inhibition on the CAN-2409-induced cytokine profile *in vitro*. Cells were treated with monotherapies or combination, and after 48 h, the conditioned media were co-cultured with peripheral blood mononuclear cells (PBMCs). After another incubation period of 72 h, supernatant was harvested for cytokine analysis (Figure 3B). The pro-tumorigenic cytokines interleukin 1β (IL-1β; combination versus control p = 0.0043, combination versus AZD6738 p = 00.0021, combination versus CAN-2409 p = 0.0061) and IL-4 (combination versus control p = 0.0001, combination versus AZD6738 p = 0.0002, combination versus CAN-2409 p = 0.0481) were significantly reduced after combination treatment compared with untreated control and monotherapies. We also observed a trend toward diminished expression of the pro-tumorigenic cytokines IL-6, IL-10, and granulocyte-macrophage colony-stimulating factor (GM-CSF; data not shown). A general decreasing trend was also observed in the anti-tumorigenic cytokines interferon gamma (IFN-γ), IL-12, and IL-13 (Figure 3C); IL-2 did not exhibit significant alterations (data not shown). These data suggest that ATR inhibition could suppress inflammatory cytokines induced by CAN-2409.

Altered immune cell-tumor cell interaction after combined treatment with CAN-2409 and ATR inhibition

The immunogenic effects of CAN-2409 are mediated by $CD8^+$ T cells[26] and natural killer (NK) cells,[31] eventually culminating in long-term anti-tumor immunity. The NKG2D receptor is expressed on NK cells and $CD8^+$ T cells; the binding to its ligands MICA/MICB—which are upregulated on tumor cells as a response to DNA damage—mediates tumor cell killing.[32] After combined treatment with CAN-2409 and ATR inhibition with AZD6738, the expression of MICA/MICB was significantly reduced compared with control and the monotherapies (Figure 3D).

As shown previously, CAN-2409 leads to an upregulation of PD-L1,[26] which mediates T cell exhaustion and thereby therapy resistance. The efficacy of a combined treatment of CAN-2409 and PD-1 inhibition is currently being evaluated in a clinical trial (ClinicalTrials.gov: NCT03576612), therefore characterizing the ATR-induced effects on the PD-L1 axis was imperative. Targeting the ATR-CHK1 pathway in other cancer models in the context of double-strand break (DSB)-inducing therapies, however, was shown to attenuate this effect on PD-L.[33] These results could be confirmed in our study, as DNA damage induced by CAN-2409 combined with ATR-inhibition led to significantly reduced PD-L1 expression compared with CAN-2409 monotherapy (Figure 3E). Together, these observations suggest that ATR influences the immune microenvironment in addition to its effects on DNA repair. These changes are generally consistent with a reduction in immune activation in the combination.

ATR inhibition influences abundance and composition of tumor immune infiltrates

To determine changes of the tumor microenvironment upon disruption of the ATR-CHK1 pathyway, mass cytometry by time of flight (CyTOF) of tumor-infiltrating leukocytes (TILs) was performed on cells extracted from the GL261 tumor-bearing hemispheres of mice treated with CAN-2409, ATR inhibitor (ATRi), controls, and combination. Using the PARC clustering algorithm,[34] we identified 31 independent clusters (Figure 4A) that could be assigned to 8 distinctive leukocyte populations: $CD4^+$ T cells, $CD8^+$ T cells, double-negative T cells (DNTs), regulatory T cells (Tregs), NK cells, B cells, neutrophils, and macrophages/monocytes (Figure 4B).

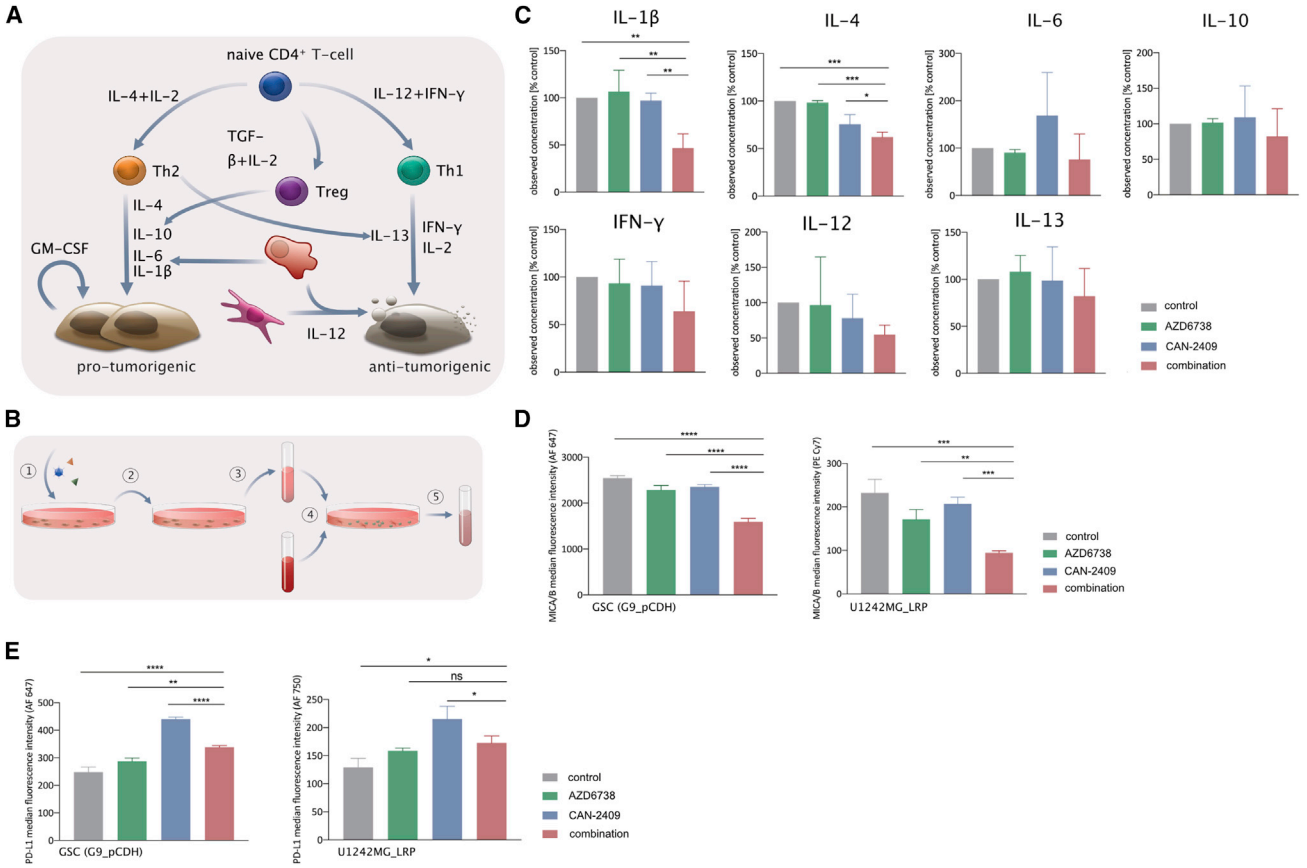

Figure 3. Altered cytokine profile and immunostimulatory receptor expression after combination treatment with CAN-2409 and ATRi

(A) Cytokine interplay in the GBM microenvironment. Cytokines contribute to the tumor microenvironment and can be characterized into pro- and anti-tumorigenic. Naïve $CD4^+$ T cells (blue) can either differentiate into Th2 cells (orange), Th1 cells (green), or Tregs. Th2 cells can produce IL-4, IL-10, IL-6, and IL-1ß, which can foster tumorigenesis, but also IL-13, which has the opposite effect.[53] Th1 triggers production of IFN-γ and IL-2, which act anti-tumorigenic. Also, macrophages (pink) and monocytes (red) influence tumor dynamics depending on the released cytokines. (B) Principle of the immune cell response and cytokine assays. G9_pCDH cells were treated with CAN-2409, AZD6738, or the combination (1), medium was changed after 24 h (2), and the cells were incubated for another 48 h. Conditioned supernatant was harvested (3) and further co-cultured with PBMCs (4). The medium was supplemented with CD3/CD28 activation beads and harvested 72 h later for the cytokine analysis (5), whereas immune cell response assays received CD3/CD28 activation beads 48 h after PBMC seeding, following further incubation time for 72 h before analysis of cell viability. (C) ATR inhibition alters the CAN-2409-induced cytokine profile. Pro-tumorigenic cytokines IL-1β and IL-4 were significantly reduced after combination treatment compared with untreated control and monotherapies. Other pro-tumorigenic cytokines like IL-6, IL-10, and GM-CSF were also attenuated, as well as the anti-tumorigenic cytokines IFN-γ, IL-12, and IL-13. (D) Reduced MICA/MICB expression after combined CAN-2409 and ATRi. Flow cytometry data of G9-pCDH and U1242_LRP. Concomitant ATR inhibition with AZD6738 leads to a significant decrease of MICA/B on both G9_pCDH and U1242_LRP cells. (E) Reduced PD-L1 expression after combined CAN-2409 and ATRi. Flow cytometry data of G9-pCDH and U1242_LRP showing significant reduction of PD-L1 expression after combinatorial treatment compared with CAN-2409 monotherapy.

We observed significant increases of $CD4^+$ T cells and B cells as well as a gain of NK cells, Tregs, and DNTs after combined treatment compared with CAN-2409, while the abundance of $CD8^+$ T cells, neutrophils, and macrophages/monocytes was reduced (Figure 4C).

$CD8^+$ T cells consist of 3 separate subclusters: pC05 ($CD86^+Ly6c^+$), pC19 ($CD86^+CD39^+$granzyme $B^+CD68^+Ly6c^+CD69^+$) and pC29 (granzyme $B^+CD196^+VEGFR1^+$) (Figures 5A, 5B, and S3). Principally, cluster pC05 is granzyme $B^{low}/Ly6c^{high}$, therefore sharing features of central memory T cells (T_{CM}s), while clusters pC19 and pC29 can be considered more as effector memory cells (T_{EM}s) due to their high expression of granzyme B (Figure S3). A closer examination of marker expression (also in accordance with marker expression in Figure S3) between the subclusters showed reduced expression of granzyme B as well as the exhaustion markers CD152, PD-1, and LAG3 after combined treatment over all clusters (Figure 5C). Significance analysis of microarray (SAM) analysis of the $CD8^+$ T cell population showed significant marker expression changes between treatments for CD45, granzyme B, and CD39, with CD45 and CD39 being increased in the combination treatment compared with CAN-2409 and a statistically significant reduction of granzyme B in the combination cohort compared with control or ATRi monotherapy (Figure 5D).

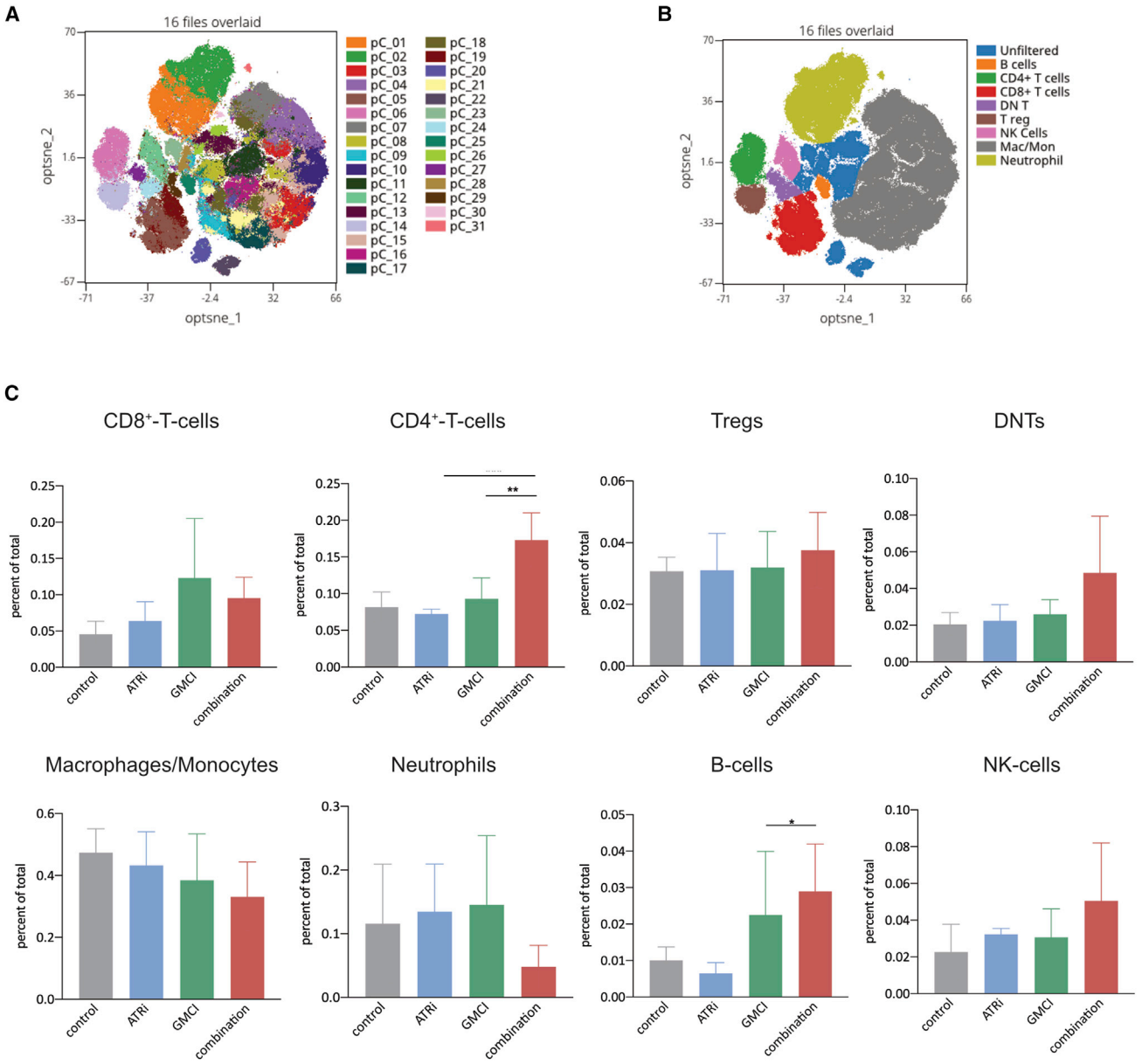

Figure 4. ATRi changes the CAN-2409-associated immune cell composition *in vivo*

A tSNE map of CyTOF-identified leukocyte subpopulations of all samples. Plot showing 31 distinct subpopulations of all 16 samples from untreated control, AZD6738, CAN-2409, and combination animal cohorts. n = 4 per group. (B) tSNE plot of leukocyte populations. CyTOF analysis of all samples showing the distribution and frequency of B cells, CD4+ T cells, CD8+ T cells, double-negative T cells (DNTs), Tregs, NK cells, macrophages/monocytes, and Neutrophils. (C) Therapy-associated changes in leukocyte distribution. After combination treatment in relation to CAN-2409, significant increases of $CD4^+$ T cells and B cells as well as a trend toward enhanced NK cells was noted. In contrast, $CD8^+$ T cells, neutrophils, and macrophages were decreased after CAN-2409 +ATRi.

$CD4^+$ T cells comprise one cluster only, which is defined as $CD44^+CD86^+CD73^+$. After combinatorial treatment, downregulation of the exhaustion markers PD-1, CD152 (CTLA-4), and LAG3 was observed. Compared with CAN-2409 monotherapy, combined ATR inhibition with CAN-2409 is associated with increased expression of the activation and memory T cell marker CD44[35] in combination with the simultaneous upregulation of CD69 and the downregulation of CD62L and CD196, suggesting a shift toward a T_{EM} profile (Figure 5E).

According to SAM analysis, $CD4^+$ T cells show significant marker expression changes for CD45, CD38, CD39, and CD152. While the

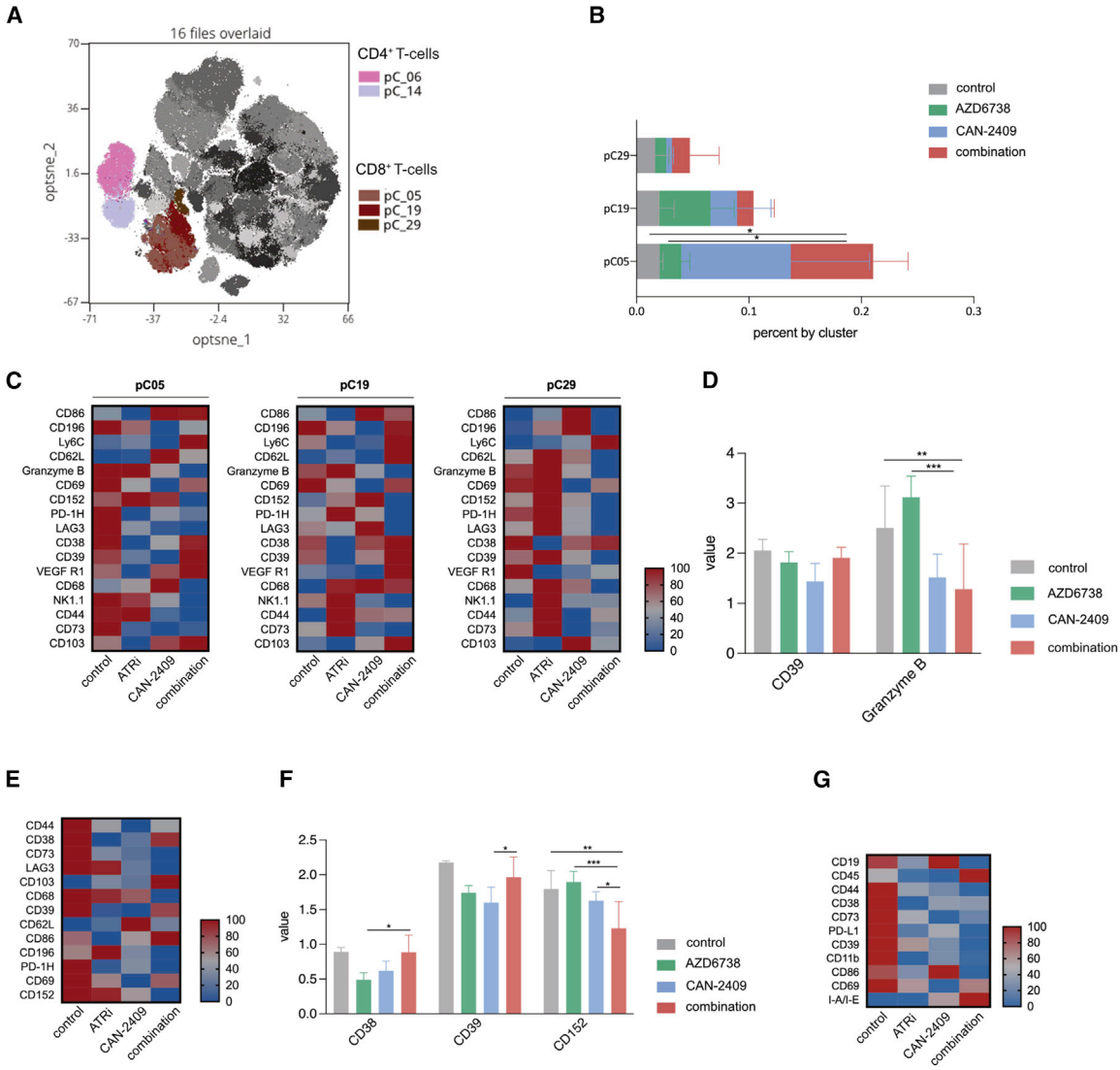

Figure 5. Combination treatment increases abundance and changes marker expression of CD4⁺ T cells and B cells

(A) Overlay of T cell clusters on tSNE cell map with focus on $CD4^+$ and $CD8^+$ T cells. $CD4^+$ T cells consist of the two subpopulations pC_06 and pC_14, with the latter being Tregs, while $CD8^+$ T cells consist of the three subpopulations pC_05, pC_19, and pC_29. (B) Distribution analysis of $CD8^+$ T cell subclusters after treatment. Most abundant subcluster is pC_05, showing significant changes after combination treatment compared with control ($p = 0.0228$) and AZD6738 ($p = 0.02$). (C) Heatmaps for markers of interest after treatment in $CD8^+$ T cell subclusters. (D) Significantly altered markers in $CD8^+$ T cells. SAM analysis demonstrated significant changes in the expression pattern of CD39 and granzyme B. Secondary analysis with two-way ANOVA and Dunnett's multiple comparisons test showed significant changes in expression of granzyme B in combination compared with control ($p = 0.0082$) and ATRi monotherapy ($p = 0.0001$). (E) Heatmap for markers of interest after treatment in $CD4^+$ T cell subclusters. (F) Significantly altered markers in $CD4^+$ T cells. SAM analysis demonstrated significant changes in the expression pattern of CD38 (combination versus ATRi $p = 0.0264$), CD39 (combination versus CAN-2409 $p = 0.0421$), and CD152 (combination versus control $p = 0.0011$, combination versus ATRi $p = 0.0001$, combination versus CAN-2409 $p = 0.0247$). (G) Heatmap for markers of interest after treatment in B cell subclusters.

patterns of CD45, CD38, and CD39 point to increased expression after combination treatment compared with CAN-2409, the opposite is observed for CD152 (Figure 5F). A more immunogenic profile, together with increased CD38 and CD39 might act opposingly, therefore no absolute subsumption can be made. These changes indicate potential dysfunctionality of these cells.

The macrophage population (Figures 6A and 6B) is distributed into 12 subpopulations, among which the clusters pC03 ($CD38^+CD39^+$ $PD\text{-}L1^+CD172a^+F4/80^+CD206^+CD86^+$), pC04 ($CD39^+PD\text{-}L1^+Arg\text{-}1^+CD86^+$MHC class $II^+Ly6\ c^+$), pC07 ($CD86^+Ly6c^+$), and pC08 (major histocompatibility complex [MHC] class II^+) are considered the most abundant. After combination treatment with CAN-2409

with ATR inhibition, we predominantly observed a reduction of pro-tumorigenic CD206 and VEGFR1 and an increase of PD-L1, while the anti-tumorigenic marker CD38 mainly was upregulated and the co-stimulatory molecule CD86 reduced (Figure 6C). These changes point to a less tumorigenic macrophage profile.

Neutrophils clustered into 4 subpopulations, among which pC01 and pC02 are the most abundant (Figures 6D and 6E) and show differential marker expression (Figures S2 and 6F). In both subclusters, the combined treatment with CAN-2409 and AZD6738 is associated with a reduced expression of CD44, Ly6G, CD172a, F4/80, and CD62L compared with CAN-2409 monotherapy, while the opposite was observed for CD196 (Figure 6F).

NK cells comprise one cluster that is defined by elevated expression of CD45, NK1.1, and Granzyme B (Figures S2 and 6G), with NK1.1 and granzyme B being downregulated in the combination treatment. Granzyme B proved to be significantly changed according to SAM analysis (Figure 6H).

Taken together, the immune cell composition of the tumor microenvironment is altered by the combined treatment of CAN-2409 and ATRi, i.e., an increase of $CD4^+$ T cells, B cells, and NK cells and a decrease of neutrophils and macrophages, suggesting a more favorable immune profile, which is backed by a reduced expression of exhaustion markers CD152, PD-1, and Lag3 in $CD4^+$ and CD8+ T cells and an overall less pro-tumorigenic macrophage profile (reduced CD206 and VEGFR1 expression, increased CD38 expression). However, we also observed an increase in Tregs as well as a reduction of $CD8^+$ T cells and reduced expression of granzyme B in NK cells—cells that are crucial for the CAN-2409-mediated effects. Therefore, the immunogenic alterations caused by the combination of ATRi and CAN-2409 are complex. After all, the CyTOF data suggest that ATRi blocks, to some extent, the immunostimulatory effects of CAN-2409 by modulating the immune cell composition and the functional immune cell status.

DISCUSSION

DDR-signaling disruption—e.g., ATR inhibition—can enhance cytotoxic effects of DNA-damage-inducing agents and might thereby amplify their therapeutic efficiency. On the other hand, DDR signaling triggers immune activation.[36] This study sought to characterize the effect of DDR-signaling disruption with ATR inhibitor AZD6738 on the efficiency of gene-suicide therapy approaches utilizing the replication-deficient CAN-2409 with GCV.

CAN-2409 has been shown to significantly prolong survival in patients with GBM;[25] its mode of action includes cytotoxic tumor cell death by induction of DNA damage and consecutive immunogenic tumor cell killing by locally recruited and activated immune cells. AZD6738 (ceralasertib) is a selective ATR inhibitor that is currently in >30 clinical trials for various malignancies and can be successfully delivered to the brain,[27] therefore making it a promising therapeutic combination partner for the treatment of GBM.

In vitro, combined treatment with ATRi and CAN-2409 resulted in elevated DNA damage, synergistically increased tumor cell killing, and reduced expression of PD-L1 on tumor cells. Assessment of immunogenicity revealed complex modifications with significantly diminished pro-tumorigenic cytokines but also decreased expression of NK-cell-activating ligand MICA/B. *In vivo*, CAN-2409, with concomitant DDR-signaling disruption, proved to significantly prolong median survival but did not provide additional survival benefit in a second tumor-re-challenge experiment. Mass cytometry of TILs revealed significantly increased abundance of $CD4^+$ T cells and B cells as well as depleted macrophage and neutrophil populations.

In our data, we show that DDR-signaling disruption with AZD6738 in combination with CAN-2409 significantly potentiates DNA damage as measured by γH2AX foci and consecutive significant increments in cytotoxic cell death (Figure 1). This correlates with previous observations: AZD6738 led to increased tumor cell death in combination with other DNA-damage-inducing agents like cisplatin,[29,37,38] gemcitabine,[39] and radiation.[40] The combination of CAN-2409 and AZD6738 successfully prolonged immediate survival *in vivo* (Figure 2B) but did not amplify CAN-2409-induced long-term anti-tumor-immunity (2 days), prompting a detailed analysis of immunological alterations following this treatment regimen.

Cytokine analysis might suggest anti-tumorigenic modifications after combined treatment with CAN-2409 and ATRi. Both pro-tumorigenic IL-4 and IL-1β were significantly reduced, and a trend toward a similar dynamic was seen for IL-6, IL-10, and GM-CSF, suggesting a fortified anti-glioma response.[41–43] On the other hand, we also observed reduced expression of IFN-γ, IL-12, and IL-13, which might create a less inflammatory microenvironment that could be responsible for the decrease of immune memory as seen in the tumor-re-challenge experiment. Nevertheless, the corresponding conclusions have to be treated with caution, as the results gained from *in vitro* experiments naturally cannot depict the entire complex interactions of the tumor microenvironment.

Disruption of the ATR-CHK1 signaling cascade under concomitant DNA-damage-inducing therapies has been shown to alter the tumor microenvironment by changing proportions of both innate and adaptive immune cells. Here, we observed significant increases in T and B cells, while glioma-propagating neutrophil and macrophage populations were diminished.

In a model of colorectal cancer and radiation treatment, Vendetti et al. observed a time-dependent reduction of $CD8^+$ T cells with a simultaneous increase of the $CD8^+$/Treg ratio and minimized expression of the exhaustion markers PD-1, LAG-3, and TIM-3.[33] Similar changes on the tumor microenvironment were noted after combinatorial treatment with AZD6738 and radiation in a hepatocellular tumor model;[44] the authors reported that combined treatment resulted in a higher proportion of $CD8^+$ T cells, while the opposite was observed for Tregs. Another study investigated the effects of

combined AZD6738 and radiation in a HPV-induced lung tumor cell line, which led to an increase of NK cells as well as $CD3^+$ T cells and Tregs.[40] Our data confirm these results as we also noticed a gain of Tregs, DNTs ($CD3^+CD4^-CD8^-$), and NK cells (all non-significant). Other than previously reported, we additionally observed a significant increment of B cells and $CD4^+$ T cells and a reduced abundance of $CD8^+$ T cells compared wtih CAN-2409. Previous reports proved that increased $CD4^+$ T cell proportions in a prostate cancer model after combined CAN-2409/GCV and radiation[45] were associated with decreased tumor growth. In the context of CAN-2409/GCV-induced T cell recruitment and activation, B cells were shown to be crucial mediators.[46]

Functionally, we observed a predominant shift towards a pro-immunogenic profile in cell populations of both innate and adaptive immune systems after combined treatment. The phenotype of macrophages can be classified as pro- and anti-tumorigenic based on marker expression.[47] Here, we observed complex alterations with a decrease of pro-tumorigenic CD206, arginase-1, and VEGF-R1, while PD-L1 expression was increased, after combined treatment with AZD6738. The pro-tumorigenic CD86 was mainly reduced, while the immunosuppressive CD38 and CD39 were upregulated in the same condition. Combined CAN-2409 and ATRi also resulted in an accumulation of NK cells, suggesting enforced immunogenicity; nevertheless, diminished expression of NK cell activation marker granzyme B was noticed. In $CD4^+$ T cells, we detected a trend toward an activated state, including upregulation of CD38[48] and downregulation of CD152.[49] However, an increase in expression of Treg marker CD39 was noted,[50,51] also corresponding to the observed gain of Tregs. Concordant to the reports of Vendetti et al.,[33] combined treatment with AZD6738 and CAN-2409 was associated with diminished expression of exhaustion markers PD-1, LAG3, and also CTLA-4 (Figure 5C), underlining either a potential gain in immunogenicity or reduced activation. Both fluorescence-activated cell sorting (FACS) and CyTOF data (Figures 3C and 5C) pointed toward a downregulation of the PD-1/PD-L1 axis after combined treatment with CAN-2409 and ATR inhibition. Although PD-1/PD-L1 signaling is considered one of the main drivers of T cell exhaustion, it is relevant for the adequate formation and functioning of $CD8^+$ memory T cells[52] and might explain the reduced long-term anti-tumor immunity observed in the *in vivo* tumor-re-challenge experiment. Also, the changes of and within the $CD8^+$ T cell population might explain the reduction of inflammation in the tumor microenvironment in the combination group. As a limitation, almost all the animals in the survival study—and at a more distinct manifestation in the re-challenge experiment—had a triventricular hydrocephalus that progressed. These alterations might have contributed to the reduced median survival of combination-treated animals in the tumor-re-challenge study.

The NKG2D ligands MICA and MICB have been shown to be upregulated upon DNA damage. Although CAN-2409, in combination with ATR inhibition, leads to an increased DNA damage (Figures 1A and 1B), we observed reduced levels of MICA and MICB after this treatment compared with CAN-2409 (Figure 3D). Friese et al.[53] demonstrated that the expression of NKG2D and its ligand MICA in malignant gliomas is diminished as a result of tumor growth factor ß (TGF-ß) signaling, which has been shown to be enhanced by ATM activation as a result of DDR[54] and might explain the observed reduced expression of MICA and MICB, as AZD6738 is selective for ATR only. The reduced NKG2D levels after combinatorial treatment might add to the attenuated *in vivo* long-term immunity as observed in the *in vivo* re-challenge experiment.

Taken together, our findings demonstrate that ATR inhibition is a potent enhancer of CAN-2409 cytotoxic features *in vitro* and *in vivo* and can be a useful therapeutic add on for treatment of GBM. As the disruption of ATR in context of DSB-inducing immunotherapies has complex ramifications on composition and function of immune cells, further studies are required to optimize the therapeutic approach, i.e., sequence of therapies, dosage, and combination partners, to fully exploit the remarkable cytotoxic as well as the immunological antitumor effects.

MATERIALS AND METHODS

Cell culture and reagents

For *in vitro* experiments, we used the patient-derived GBM stem-like cell line G9_pCDH,[55] as well as the long-term GBM cell line U1242_LRP. For *in vivo* studies, murine GBM GL261fluc cells were used. All cells were cultured at 37°C, 5% CO_2, with either Dulbecco's modified Eagle's medium (Life Technologies) containing 10% heat-inactivated fetal bovine serum, Plasmocin (ant-mpp, Invivogen), and Primocin (ant-pm1, Invivogen) (i.e., DMEM complete) or with Neurobasal Medium (Life Technologies) containing B27 (Invitrogen), 1% Glutamax (Invitrogen), 20 ng/mL EGF (Peprotech), 20 ng/mL FGF (Peprotech), Primocin (ant-pm1, Invivogen), and Plasmocin (ant-mpp, Invivogen). Cells were regularly tested for mycoplasma infection. GCV and the HSV-tk-containing virus CAN-2409 were provided by Candel Therapeutics (Needham, MA, USA). CAN-2409 has been described in previous publications.[26] For the *in vitro* experiments, cells were treated with CAN-2409 (multiplicity of infection [MOI] 100), GCV (10 μg/mL), AZD6738, and AZD1390 (both Selleckchem) at the corresponding half maximal inhibitory concentration (IC_{50}) for each drug.

Cell viability assays

5,000 tumor cells/well were seeded in complete DMEM. Treatment with the respective agents or mock was performed at the indicated concentrations 24 h after seeding. PrestoBlue cell viability reagent (Invitrogen) was added 96 h after seeding in accordance with the manufacturer's instructions, and readout was performed with the OmegaStar plate reader (BMG Labtech). Each experiment was performed with 2 (consisting of 5 technical replicates) or 3 biological replicates (consisting of 3 technical replicates).

Synergistic or additive treatment effects were assessed in accordance with previous reports.[56–58] In brief, measured cell viability values of each condition were normalized to the untreated control and thereby

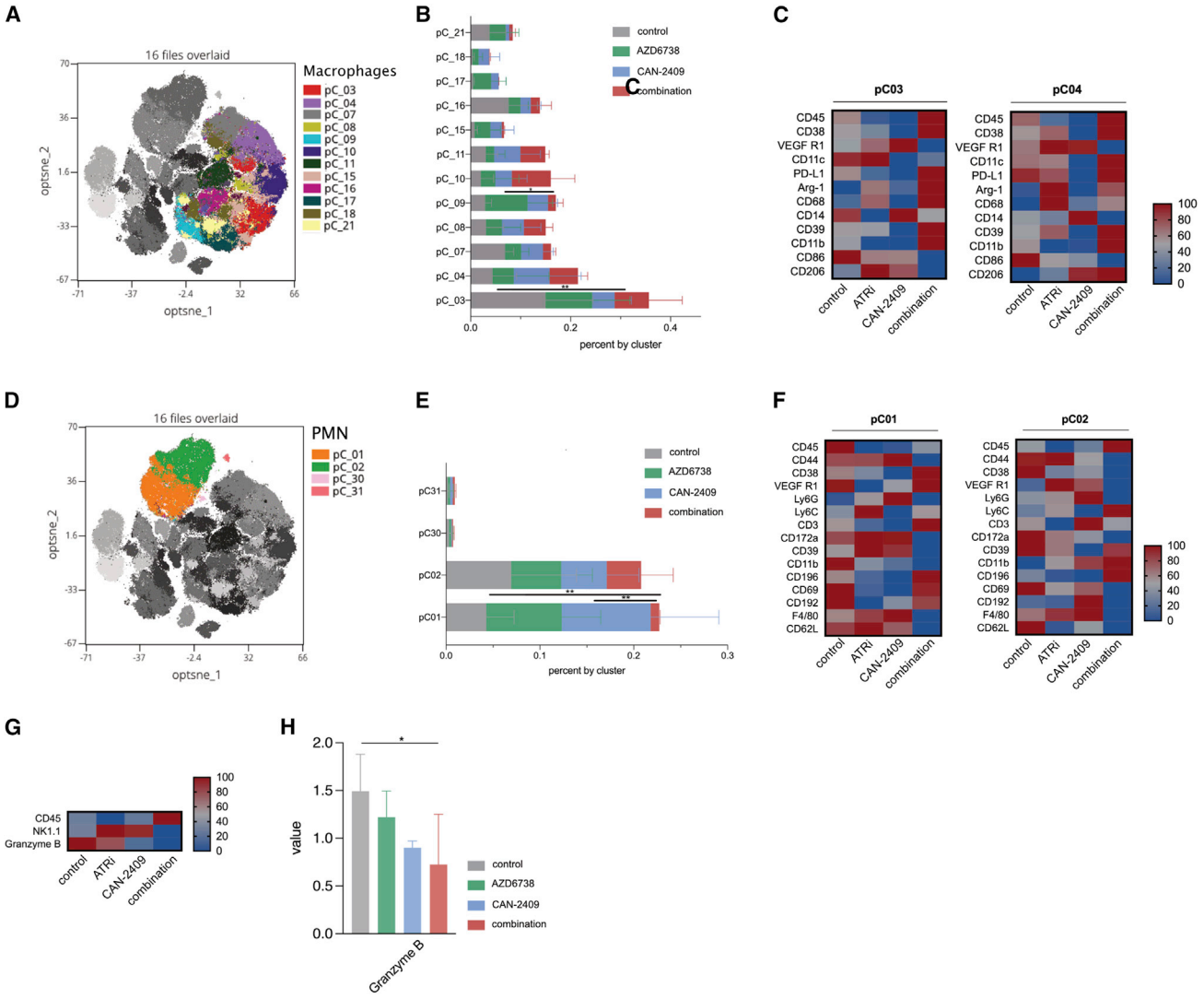

Figure 6. Combined ATRi and CAN-2409 leads to reduction of macrophages and neutrophils while reducing granzyme B expression in NK cells

(A) Overlay of macrophage clusters on tSNE cell map. Macrophages consist of the 12 subpopulations pC_03, pC_04, pC_07, pC_08, pC_09, pC_10, pC_11, pC_15, pC_16, pC_17, pC_18, and pC_21. (B) Distribution analysis of macrophage subclusters after treatment. Most abundant subcluster is pC_03, showing significant changes after combination treatment compared with control ($p = 0.0035$). (C) Heatmap for markers of interest after treatment in macrophage subclusters. (D) Overlay of neutrophil clusters on tSNE cell map. The neutrophil cluster consists of the 4 subpopulations pC_01, pC_02, pC_30, and pC_31. (E) Distribution analysis of neutrophil subclusters after treatment. Most abundant subclusters are pC_01 and pC_02, the first showing significant changes after combination treatment compared with ATRi ($p = 0.0076$) and CAN-2409 ($p = 0.0012$). (F) Heatmap for markers of interest after treatment in neutrophil subclusters. (G) Heatmap for markers of interest after treatment in NK cells. (H) Significantly altered granzyme B in NK cells. SAM analysis demonstrated significant changes in the expression pattern of granzyme B, with the lowest marker expression after combination treatment. Secondary statistical analysis with two-way ANOVA and Dunnett's multiple comparisons test showed significance in the contrast combination versus control ($p = 0.0261$).

converted to percentage values (observed values). Predicted values of the combinatorial treatments were defined as the arithmetical product of the respective monotherapies. To assess synergy in the combination treatment, observed values of the combinations were compared with the respective predicted values. A treatment was determined to be synergistic if the observed value was less than the predicted value.[58]

Flow cytometry (FACS)

1,000,000 G9_pCDH or 500,000 U1242_LRP cells/well were seeded in complete DMEM in 6-well plates in triplicates and immediately infected with CAN-2409 MOI 100/well. For all experiments, two biological replicates or a time course was performed. Treatment with GCV (10 μg/mL), AZD6738 (IC_{50}), AZD1390 (IC_{50}), or combination was performed 24 h after seeding. 24 and/or 48 h after treatment, cells

were harvested, washed, and stained with the corresponding antibodies PD-L1 (Alexa Fluor 647, 750 R&D Systems FAB1561R-025, 5 μL/test) or MICA/MICB (clone 6D4 Alexa Fluor 647, PE/Cyanine7, Biolegend) and LIVE/DEAD Fixable Violet Dead Cell Stain Kit (#L34963, Thermo Fisher Scientific) and fixed using 4% PFA. For intracellular staining with γH2AX(Ser139) (clone 2F3, fluorescein isothiocyanate [FITC], Alexa Fluor 647 Biolegend), cells were first fixed with 4% PFA followed by antibody staining in permeabilization medium (Thermo Fisher Scientific) for 40 min at room temperature. Flow cytometry was performed with BD Fortessa or BD Aria, and 10,000 events were counted. Data were analyzed using FlowJo software (Bio-Rad).

Western blot

G9_pCDH and U1242_LRP cells were seeded and treated under the same conditions as mentioned above and harvested after 24 or 48 h of incubation. Treatment with GCV (10 μg/mL), AZD6738 (1 μM), or combination was performed 24 h after seeding. 24 and/or 48 h after treatment, cells were harvested. Generation of protein lysates was performed with radioimmunoprecipitation assay (RIPA) lysis and extraction buffer (Thermo Fisher Scientific) together with Halt Protease Inhibitor Cocktails (Thermo Fisher Scientific). Protein concentration was measured with the Pierce BCA Protein Assay Kit (Thermo Fisher Scientific). Protein segregation with SDS-PAGE was done utilizing 4%–20% Mini-PROTEAN TGX Precast Protein Gels (Bio-Rad) or 4–20% Criterion™ TGX™ Gels (Bio-Rad) and 1× Tris/Glycine/SDS buffer (Bio-Rad), followed by membrane transfer with 1× Tris/Glycine buffer (Bio-Rad, #1610771) with 20% methanol. The following primary antibodies (all purchased from Cell Signaling Technologies) were used: CHK1 (2G1D5, #2360 S), phospho-Chk1 (Ser345) (#2348), and phospho-Chk1 (Ser317) (#2344). As secondary antibodies, anti-rabbit immunoglobulin G (IgG) HRP-linked antibody (#7074 s, Cell Signaling Technologies) and ECL anti-mouse IgG HRP-linked antibody (#LNA931 V/AH, GE Healthcare) were used. Alexa Fluor 488-labeled anti-GAPDH served as control (#sc-365062, Santa Cruz). Analysis was carried out by incubation with Super Signal West Pico Plus Chemiluminescent Substrate (#34850, Thermo Fisher Scientific).

Cytokine analysis

200,000 G9_pCDH cells per well were seeded in triplicates and treated with CAN-2409, GCV, and AZD6738 as indicated. A medium change was performed 24 h later. Supernatant media were harvested 48 h later and co-incubated with 40,000 PBMCs; Dynabeads Human T-Activator CD3/CD28 beads (Gibco) were added in a 1:1 ratio. PBMC-conditioned media were harvested 72 h later and stored at −80°C. Samples were analyzed for their cytokine concentration, including GM-CSF, IFN-γ, IL-1β, IL-2, IL-4, IL-5, IL-6, IL-8, IL-10, IL-12(p70), IL-13, MCP-1, and TNF-α (HDF13 panel, Eve Technologies, Calgary, AB, Canada).

In vivo survival studies

For *in vivo* survival studies, 7- to 8-week-old female albino C57/BL6 mice were purchased from Envigo. After a 2 week settling-in period, 100,000 GL261fluc cells were injected intracranially in 2 μL HBSS 2 mm right lateral, 1 mm frontal to the bregma, and 3 mm deep. 7 or 9 days later, 3 μL CAN-2409 (2×10^8 vector particles [vp]/μL) sham was injected into the same location. GCV (20 mg/kg body weight) was administered twice daily intraperitoneally and AZD6738 (50 mg/kg body weight) once daily orally for a total of 7 days. Each cohort consisted of 6 mice. Animal distribution was based on body weight and bioluminescence signal. Treatment was performed in one session, and animals were held in the same space. Endpoint for sacrificing the mice was considered either a weight loss equal of more than 20%, onset of neurological symptoms, or signs of pain and distress. The experiment was terminated 125 days after tumor implantation, and the curves were right censored.

A tumor-re-challenge experiment was performed with long-term-surviving animals on day 125 after the initial tumor implantation (long-term survivors: CAN-2409 n = 3, combination n = 3), and 16- to 18-week-old tumor-naive albino C57/BL6 served as control. 100,000 GL261fluc cells were injected intracranially into the contralateral hemisphere similar to the first surgery. No therapy was administered. Endpoint criteria were considered again as a weight loss >20%, onset of neurological symptoms, or signs of pain and distress. Curves were right censored 63 days after tumor implantation. All animal studies were approved by BWH Center for Comparative Medicine IACUC

Bioluminescence imaging

To verify successful GL261fluc tumor cell implantation, animals under isoflurane anesthesia were injected with 100 μL 30 mg/mL D-Luciferin (#LUCK-1G, Gold Biotechnology) and imaged using the Perkin-Elmer IVIS Lumina 3.

MRI

MRI was performed on days 18, 25, and 31 after tumor implantation to monitor tumor growth and response to therapy in the survival study. For the tumor-re-challenge experiment with, MR images were acquired on days 14, 21, and 28 after the second tumor implantation. Mice were anaesthetized with isoflurane for the time of the MRI study. MRI was performed with the Bruker BioSpec 3 T utilizing the setup "mouse body RF coil with respiratory monitoring." Images were acquired using the T2_TurboRARE sequence with the following settings: TE: 47.73 ms, TR: 4,993.715 ms, rare factor: 8, averages: 3, slice thickness: 0.5 mm, slicer orientation: axial, field of view: 20 * 20 mm, and resolution: 0.078 * 0.078 mm. Tumor volume was analyzed using the JiveX DICOM Viewer (VISUS Health IT GmbH, Bochum, Germany).

Isolation of murine TILs

For the isolation of TILs, animals were treated as described before and euthanized 21 days after tumor implantation. The hemisphere harboring the tumor was collected, and the mouse tumor dissociation kit (Miltenyi Biotec) was used for isolation of TILs according to the manufacturer's instructions. Harvested leukocytes were stored at −80°C until further use.

CyTOF

All samples were thawed in a 37°C water bath for 3 min and then mixed with 37°C thawing media containing: RPMI Medium 1640 (Life Technologies #11875-085) supplemented with 5% heat-inactivated fetal bovine serum (Life Technologies #16000044); 1 mM GlutaMAX (Life Technologies #35050079); antibiotic-antimycotic (Life Technologies #15240062); 2 mM MEM non-essential amino acids (Life Technologies #11140050); 10 mM HEPES (Life Technologies #15630080); 2.5×10^{-5} M 2-mercaptoethanol (Sigma-Aldrich #M3148); 20 units/mL sodium heparin (Sigma-Aldrich #H3393); and 25 units/mL benzonase nuclease (Sigma-Aldrich #E1014). 100 μL aliquots of each sample post-thaw were mixed with PBS (Life Technologies #10010023) at a 1:1 ratio to be counted by flow cytometry. Between 0.5 and 1.0×10^6 cells were used for each sample. All samples were transferred to a polypropylene plate to be stained at room temperature for the rest of the experiment.

The samples were spun down and aspirated. 5 μM cisplatin viability staining reagent (Fluidigm #201064) was added for 2 min and then diluted with culture media. 16% stock paraformaldehyde (Thermo Fisher Scientific #O4042-500) dissolved in PBS was used at a final concentration of 0.2% formaldehyde for 5 min in order to fix the samples before staining. After centrifugation, mouse anti-CD16/32 antibody Fc-receptor-blocking reagent (BioLegend #101302) was used at a 1:100 dilution in CSB (PBS with 2.5 g bovine serum albumin [Sigma Aldrich #A3059] and 100 mg of sodium azide [Sigma Aldrich #71289]) for 15 min followed by incubation with conjugated surface antibodies (each marker was used at a 1:100 dilution in CSB unless stated otherwise) for 30 min. All antibodies were obtained from the Harvard Medical Area CyTOF Antibody Resource and Core (Boston, MA, USA).

16% stock paraformaldehyde dissolved in PBS was used at a final concentration of 4% formaldehyde for 10 min in order to fix the samples before permeabilization with the FoxP3/Transcription Factor Staining Buffer Set (Thermo Fisher Scientific #00-5523-00). The samples were incubated with SCN-EDTA coupled palladium-based barcoding reagents for 15 min and then were combined into a single sample. Samples were incubated in a heparin solution at 100 units/mL PBS for 15 min. Conjugated intracellular antibodies (each marker was used at a 1:100 dilution in permeabilization buffer unless stated otherwise) was added into each tube and incubated for 60 min. Cells were then fixed with 4% formaldehyde for 10 min.

To identify single-cell events, DNA was labeled for 20 min with an 18.75 μM iridium intercalator solution (Fluidigm #201192B). Samples were subsequently washed and reconstituted in Maxpar Cell Acquisition Solution (Fludigm #201241) in the presence of EQ Four Element Calibration beads (Fluidigm #201078) at a final concentration of 1×10^6 cells/mL. Samples were acquired on a Helios CyTOF Mass Cytometer (Fluidigm). The raw FCS files were normalized to reduce signal deviation between samples over the course of the acquisition time, utilizing the bead standard normalization method established by Finck et al.[59] The normalized files were then compensated with a panel-specific spillover matrix to subtract cross-contaminating signals, utilizing the CyTOF-based compensation method.[60] These compensated files were then deconvoluted into individual sample files using a single-cell-based debarcoding algorithm.[61] From there, files were uploaded to OMIQ. In OMIQ, events were cleaned up using Gaussian parameters. These cleaned up files were gated to remove normalization beads and to select live singlets. Due to the high variability of cell counts between samples, no downsampling was performed, and all events were analyzed. These live singlets were run through a principal-component analysis (PCA) for pre-embedding for an opt-SNE dimensionality reduction.[62] From there, events were clustered using PARC[34] to identify populations based on marker expression. Statistically different clusters between groups were identified using the multiclass setting of SAM.[39]

Data and materials availability

Data are available upon request from sean_lawler@brown.edu. All relevant data to the study are included in the article or uploaded as supplemental information. sean_lawler@brown.edu

SUPPLEMENTAL INFORMATION

Supplemental information can be found online at https://doi.org/10.1016/j.omto.2022.07.009.

ACKNOWLEDGMENTS

The authors thank Candel Therapeutics (Needham, MA, USA) for providing CAN-2409 and GCV used in this study. We also thank the Else Kröner Fresenius Forschungskolleg (2015_Kolleg_14) for partially funding this work (to G.T.). This study was also funded by NCI P01CA069246 and by NCI R50 CA243706-02 (MON).The graphical abstract was created with BioRender.com (agreement number BB246QKYKS).

AUTHOR CONTRIBUTIONS

Study conceptualization and design, M.S.K., S.E.L., E.A.C., J.A.L., and M.S.H.; methodology, M.S.K., M.O.N., M.Z., A.M.G., K.S., and J.A.L.; investigation, M.S.K., S.E.L., and E.A.C.; visualization, M.S.K. and A.M.G.; funding acquisition, S.E.L., E.A.C., and G.T.; project administration, M.S.K., S.E.L., and E.A.C.; supervision, S.E.L., E.A.C., and J.A.L.; writing – original draft, M.S.K. and S.E.L.; writing – review & editing, M.S.K., S.E.L., E.A.C., M.Z., M.O.N., E.A.-C., L.K.A., B.W.G., F.B., P.P.T., K.S., M.S.H., J.A.L., and G.T.

DECLARATION OF INTERESTS

None declared.

REFERENCES

1. Hanif, F., Muzaffar, K., Perveen, K., Malhi, S.M., and Simjee, S.U. (2017). Glioblastoma multiforme: a review of its epidemiology and pathogenesis through clinical presentation and treatment. Asian Pac. J. Cancer Prev. *18*, 3–9.

2. Stupp, R., Mason, W.P., van den Bent, M.J., Weller, M., Fisher, B., Taphoorn, M.J.B., Belanger, K., Brandes, A.A., Marosi, C., Bogdahn, U., et al. (2005). Radiotherapy plus concomitant and adjuvant temozolomide for glioblastoma. N. Engl. J. Med. *352*, 987–996.

3. Hodges, T.R., Ott, M., Xiu, J., Gatalica, Z., Swensen, J., Zhou, S., Huse, J.T., de Groot, J., Li, S., Overwijk, W.W., et al. (2017). Mutational burden, immune checkpoint expression, and mismatch repair in glioma: implications for immune checkpoint immunotherapy. Neuro. Oncol. *19*, 1047–1057.

4. Medikonda, R., Dunn, G., Rahman, M., Fecci, P., and Lim, M. (2020). A review of glioblastoma immunotherapy. J. Neurooncol. *151*, 41–53.

5. Jackson, C., Ruzevick, J., Phallen, J., Belcaid, Z., and Lim, M. (2011). Challenges in immunotherapy presented by the glioblastoma multiforme microenvironment. Clin. Dev. Immunol. *2011*, 732413.

6. Gilbert, M.R., Dignam, J.J., Armstrong, T.S., Wefel, J.S., Blumenthal, D.T., Vogelbaum, M.A., Colman, H., Chakravarti, A., Pugh, S., Won, M., et al. (2014). A randomized trial of bevacizumab for newly diagnosed glioblastoma. N. Engl. J. Med. *370*, 699–708.

7. Chinot, O.L., de La Motte Rouge, T., Moore, N., Zeaiter, A., Das, A., Phillips, H., Modrusan, Z., and Cloughesy, T. (2011). AVAglio: phase 3 trial of bevacizumab plus temozolomide and radiotherapy in newly diagnosed glioblastoma multiforme. Adv. Ther. *28*, 334–340.

8. Reardon, D.A., Fink, K.L., Mikkelsen, T., Cloughesy, T.F., O'Neill, A., Plotkin, S., Glantz, M., Ravin, P., Raizer, J.J., Rich, K.M., et al. (2008). Randomized phase II study of cilengitide, an integrin-targeting arginine-glycine-aspartic acid peptide, in recurrent glioblastoma multiforme. J. Clin. Oncol. *26*, 5610–5617.

9. Stupp, R., Hegi, M.E., Gorlia, T., Erridge, S.C., Perry, J., Hong, Y.-K., Aldape, K.D., Lhermitte, B., Pietsch, T., Grujicic, D., et al. (2014). Cilengitide combined with standard treatment for patients with newly diagnosed glioblastoma with methylated MGMT promoter (CENTRIC EORTC 26071-22072 study): a multicentre, randomised, open-label, phase 3 trial. Lancet Oncol. *15*, 1100–1108.

10. Weller, M., Butowski, N., Tran, D.D., Recht, L.D., Lim, M., Hirte, H., Ashby, L., Mechtler, L., Goldlust, S.A., Iwamoto, F., et al. (2017). Rindopepimut with temozolomide for patients with newly diagnosed, EGFRvIII-expressing glioblastoma (ACT IV): a randomised, double-blind, international phase 3 trial. Lancet Oncol. *18*, 1373–1385.

11. Reardon, D.A., Lassman, A.B., van den Bent, M., Kumthekar, P., Merrell, R., Scott, A.M., Fichtel, L., Sulman, E.P., Gomez, E., Fischer, J., et al. (2017). Efficacy and safety results of ABT-414 in combination with radiation and temozolomide in newly diagnosed glioblastoma. Neuro. Oncol. *19*, 965–975.

12. Stupp, R., Wong, E.T., Kanner, A.A., Steinberg, D., Engelhard, H., Heidecke, V., Kirson, E.D., Taillibert, S., Liebermann, F., Dbalý, V., et al. (2012). NovoTTF-100A versus physician's choice chemotherapy in recurrent glioblastoma: a randomised phase III trial of a novel treatment modality. Eur. J. Cancer *48*, 2192–2202.

13. Omuro, A., Vlahovic, G., Lim, M., Sahebjam, S., Baehring, J., Cloughesy, T., Voloschin, A., Ramkissoon, S.H., Ligon, K.L., Latek, R., et al. (2018). Nivolumab with or without ipilimumab in patients with recurrent glioblastoma: results from exploratory phase i cohorts of CheckMate 143. Neuro. Oncol. *20*, 674–686.

14. Hilf, N., Kuttruff-Coqui, S., Frenzel, K., Bukur, V., Stevanović, S., Gouttefangeas, C., Platten, M., Tabatabai, G., Dutoit, V., van der Burg, S.H., et al. (2019). Actively personalized vaccination trial for newly diagnosed glioblastoma. Nature *565*, 240–245.

15. Markert, J.M., Razdan, S.N., Kuo, H.C., Cantor, A., Knoll, A., Karrasch, M., Nabors, L.B., Markiewicz, M., Agee, B.S., Coleman, J.M., et al. (2014). A phase 1 trial of oncolytic HSV-1, g207, given in combination with radiation for recurrent GBM demonstrates safety and radiographic responses. Mol. Ther. *22*, 1048–1055.

16. Rubsam, L.Z., Boucher, P.D., Murphy, P.J., KuKuruga, M., and Shewach, D.S. (1999). Cytotoxicity and accumulation of ganciclovir triphosphate in bystander cells cocultured with herpes simplex virus type 1 thymidine kinase-expressing human glioblastoma cells. Cancer Res. *59*, 669–675.

17. Ewald, B., Sampath, D., and Plunkett, W. (2008). Nucleoside analogs: molecular mechanisms signaling cell death. Oncogene *27*, 6522–6537.

18. Krohne, T.U., Shankara, S., Geissler, M., Roberts, B.L., Wands, J.R., Blum, H.E., and Mohr, L. (2001). Mechanisms of cell death induced by suicide genes encoding purine nucleoside phosphorylase and thymidine kinase in human hepatocellular carcinoma cells in vitro. Hepatology *34*, 511–518.

19. Tomicic, M.T., Thust, R., and Kaina, B. (2002). Ganciclovir-induced apoptosis in HSV-1 thymidine kinase expressing cells: critical role of DNA breaks, Bcl-2 decline and caspase-9 activation. Oncogene *21*, 2141–2153.

20. Srivastava, D., Joshi, G., Somasundaram, K., and Mulherkar, R. (2011). Mode of cell death associated with adenovirus-mediated suicide gene therapy in HNSCC tumor model. Anticancer Res. *31*, 3851–3857.

21. Whartenby, K.A., Abboud, C.N., Freeman, S.M., Packman, C.H., Koeplin, D.S., Moolten, F.L., and Abraham, G.N. (1993). The "bystander effect": tumor regression when a fraction of the tumor mass is genetically modified. Cancer Res. *53*, 5274–5283.

22. Kaneko, Y., and Tsukamoto, A. (1995). Gene therapy of hepatoma: bystander effects and non-apoptotic cell death induced by thymidine kinase and ganciclovir. Cancer Lett. *96*, 105–110.

23. Vile, R.G., Castleden, S., Marshall, J., Camplejohn, R., Upton, C., and Chong, H. (1997). Generation of an anti-tumour immune response in a non-immunogenic tumour: HSVtk killing in vivo stimulates a mononuclear cell infiltrate and a Th1-like profile of intratumoural cytokine expression. Int. J. Cancer *71*, 267–274.

24. Vile, R.G., Nelson, J.A., Castleden, S., Chong, H., and Hart, I.R. (1994). Systemic gene therapy of murine melanoma using tissue specific expression of the HSVtk gene involves an immune component. Cancer Res. *54*, 6228–6234.

25. Wheeler, L.A., Manzanera, A.G., Bell, S.D., Cavaliere, R., McGregor, J.M., Grecula, J.C., Newton, H.B., Lo, S.S., Badie, B., Portnow, J., et al. (2016). Phase II multicenter study of gene-mediated cytotoxic immunotherapy as adjuvant to surgical resection for newly diagnosed malignant glioma. Neuro. Oncol. *18*, 1137–1145.

26. Speranza, M.C., Passaro, C., Ricklefs, F., Kasai, K., Klein, S.R., Nakashima, H., Kaufmann, J.K., Ahmed, A.K., Nowicki, M.O., Obi, P., et al. (2018). Neuro-Oncology cytotoxic immunotherapy and immune checkpoint blockade in glioblastoma. Neuro. Oncol. *20*, 225–235.

27. Fròsina, G., Profumo, A., Marubbi, D., Marcello, D., Ravetti, J.L., and Daga, A. (2018). ATR kinase inhibitors NVP-BEZ235 and AZD6738 effectively penetrate the brain after systemic administration. Radiat. Oncol. *13*, 76.

28. Karlin, J., Allen, J., Ahmad, S.F., Hughes, G., Sheridan, V., Odedra, R., Farrington, P., Cadogan, E.B., Riches, L.C., Garcia-Trinidad, A., et al. (2018). Orally bioavailable and blood-brain barrier-penetrating ATM inhibitor (AZ32) radiosensitizes intracranial gliomas in mice. Mol. Cancer Ther. *17*, 1637–1647.

29. Vendetti, F.P., Lau, A., Schamus, S., Conrads, T.P., O'Connor, M.J., and Bakkenist, C.J. (2015). The orally active and bioavailable ATR kinase inhibitor AZD6738 potentiates the anti-tumor effects of cisplatin to resolve ATM-deficient non-small cell lung cancer in vivo. Oncotarget *6*, 44289–44305.

30. Zhang, Y.W., Otterness, D.M., Chiang, G.G., Xie, W., Liu, Y.C., Mercurio, F., and Abraham, R.T. (2005). Genotoxic stress targets human Chk1 for degradation by the ubiquitin-proteasome pathway. Mol. Cel *19*, 607–618.

31. Hall, S.J., Sanford, M.A., Atkinson, G., and Chen, S.H. (1998). Induction of potent antitumor natural killer cell activity by herpes simplex virus-thymidine kinase and ganciclovir therapy in an orthotopic mouse model of prostate cancer. Cancer Res. *58*, 3221–3225.

32. Schmiedel, D., and Mandelboim, O. (2018). NKG2D ligands-critical targets for cancer immune escape and therapy. Front. Immunol. *9*, 2040.

33. Vendetti, F.P., Karukonda, P., Clump, D.A., Teo, T., Lalonde, R., Nugent, K., Ballew, M., Kiesel, B.F., Beumer, J.H., Sarkar, S.N., et al. (2018). ATR kinase inhibitor AZD6738 potentiates CD8+ T cell-dependent antitumor activity following radiation. J. Clin. Invest. *128*, 3926–3940.

34. Stassen, S. v, Siu, D.M.D., Lee, K.C.M., Ho, J.W.K., So, H.K.H., and Tsia, K.K. (2020). PARC: ultrafast and accurate clustering of phenotypic data of millions of single cells. Bioinformatics *36*, 2778–2786.

35. Baaten, B.J.G., Li, C.R., Deiro, M.F., Lin, M.M., Linton, P.J., and Bradley, L.M. (2010). CD44 regulates survival and memory development in Th1 cells. Immunity *32*, 104–115.

36. Nakad, R., and Schumacher, B. (2016). DNA damage response and immune defense: links and mechanisms. Front. Genet. *7*, 147.

37. Kim, H.J., Min, A., Im, S.A., Jang, H., Lee, K.H., Lau, A., Lee, M., Kim, S., Yang, Y., Kim, J., et al. (2017). Anti-tumor activity of the ATR inhibitor AZD6738 in HER2 positive breast cancer cells. Int. J. Cancer *140*, 109–119.

38. Leonard, B.C., Lee, E.D., Bhola, N.E., Li, H., Sogaard, K.K., Bakkenist, C.J., Grandis, J.R., and Johnson, D.E. (2019). ATR inhibition sensitizes HPV− and HPV+ head and neck squamous cell carcinoma to cisplatin. Oral Oncol. *95*, 35–42.

39. Wallez, Y., Dunlop, C.R., Johnson, T.I., Koh, S.-B., Fornari, C., Yates, J.W.T., Bernaldo de Quirós Fernández, S., Lau, A., Richards, F.M., and Jodrell, D.I. (2018). The ATR inhibitor AZD6738 synergizes with gemcitabine in vitro and in vivo to induce pancreatic ductal adenocarcinoma regression. Mol. Cancer Ther. *17*, 1670–1682.

40. Dillon, M.T., Bergerhoff, K.F., Pedersen, M., Whittock, H., Crespo-Rodriguez, E., Patin, E.C., Pearson, A., Smith, H.G., Paget, J.T.E., Patel, R.R., et al. (2019). ATR inhibition potentiates the radiation-induced inflammatory tumor microenvironment. Clin. Cancer Res. *25*, 3392–3403.

41. Fathima Hurmath, K., Ramaswamy, P., and Nandakumar, D.N. (2014). IL-1β microenvironment promotes proliferation, migration and invasion of human glioma cells. Cell Biol. Int. *38*, 1415–1422.

42. Nappo, G., Handle, F., Santer, F.R., McNeill, R.v., Seed, R.I., Collins, A.T., Morrone, G., Culig, Z., Maitland, N.J., and Erb, H.H.H. (2017). The immunosuppressive cytokine interleukin-4 increases the clonogenic potential of prostate stem-like cells by activation of STAT6 signalling. Oncogenesis *6*. e342-12.

43. Iwami, K., Natsume, A., and Wakabayashi, T. (2011). Cytokine networks in glioma. Neurosurg. Rev. *34*, 253–263. discussion 263-264.

44. Sheng, H., Huang, Y., Xiao, Y., Zhu, Z., Shen, M., Zhou, P., Guo, Z., Wang, J., Wang, H., Dai, W., et al. (2020). ATR inhibitor AZD6738 enhances the antitumor activity of radiotherapy and immune checkpoint inhibitors by potentiating the tumor immune microenvironment in hepatocellular carcinoma. J. Immunother. Cancer *8*, e000340.

45. Chhikara, M., Huang, H., Vlachaki, M.T., Zhu, X., Teh, B., Chiu, K.J., Woo, S., Berner, B., Smith, E.O., Oberg, K.C., et al. (2001). Enhanced therapeutic effect of HSV-tk+GCV gene therapy and ionizing radiation prostate cancer. Mol. Ther. *3*, 536–542.

46. Candolfi, M., Curtin, J.F., Yagiz, K., Assi, H., Wibowo, M.K., Alzadeh, G.E., Foulad, D., Muhammad, A.K.M.G., Salehi, S., Keech, N., et al. (2011). B cells are critical to T-cell-mediated antitumor immunity induced by a combined immune-stimulatory/conditionally cytotoxic therapy for glioblastoma. Neoplasia *13*, 947–960.

47. Guerriero, J.L. (2018). Macrophages: the road less traveled, changing anticancer therapy. Trends Mol. Med. *24*, 472–489.

48. Sandoval-Montes, C., and Santos-Argumedo, L. (2005). CD38 is expressed selectively during the activation of a subset of mature T cells with reduced proliferation but improved potential to produce cytokines. J. Leukoc. Biol. *77*, 513–521.

49. Woroniecka, K., Chongsathidkiet, P., Rhodin, K., Kemeny, H., Dechant, C., Farber, S.H., Elsamadicy, A.A., Cui, X., Koyama, S., Jackson, C., et al. (2018). T-cell exhaustion signatures vary with tumor type and are severe in glioblastoma. Clin. Cancer Res. *24*, 4175–4186.

50. Schuler, P.J., Saze, Z., Hong, C.S., Muller, L., Gillespie, D.G., Cheng, D., Harasymczuk, M., Mandapathil, M., Lang, S., Jackson, E.K., and Whiteside, T.L. (2014). Human CD4+CD39+ regulatory T cells produce adenosine upon co-expression of surface CD73 or contact with CD73+ exosomes or CD73+ cells. Clin. Exp. Immunol. *177*, 531–543.

51. Zhou, Q., Yan, J., Putheti, P., Wu, Y., Sun, X., Toxavidis, V., Tigges, J., Kassam, N., Enjyoji, K., Robson, S.C., et al. (2009). Isolated CD39 expression on CD4 + T cells denotes both regulatory and memory populations. Am. J. Transpl. *9*, 2303–2311.

52. Pauken, K.E., Godec, J., Odorizzi, P.M., Brown, K.E., Yates, K.B., Ngiow, S.F., Burke, K.P., Maleri, S., Grande, S.M., Francisco, L.M., et al. (2020). The PD-1 pathway regulates development and function of memory CD8+ T cells following respiratory viral infection. Cell Rep. *31*, 107827.

53. Friese, M.A., Wischhusen, J., Wick, W., Weiler, M., Eisele, G., Steinle, A., and Weller, M. (2004). RNA interference targeting transforming growth factor-β enhances NKG2D-mediated antiglioma immune response, inhibits glioma cell migration and invasiveness, and abrogates tumorigenicity in vivo. Cancer Res. *64*, 7596–7603.

54. Li, Y., Liu, Y., Chiang, Y.J., Huang, F., Li, Y., Li, X., Ning, Y., Zhang, W., Deng, H., and Chen, Y.G. (2019). DNA damage activates TGF-β signaling via ATM-c-cbl-mediated stabilization of the type II receptor TβRII. Cell Rep. *28*, 735–745.e4.

55. Williams, S.P., Nowicki, M.O., Liu, F., Press, R., Godlewski, J., Abdel-Rasoul, M., Kaur, B., Fernandez, S.A., Chiocca, E.A., and Lawler, S.E. (2011). Indirubins decrease glioma invasion by blocking migratory phenotypes in both the tumor and stromal endothelial cell compartments. Cancer Res. *71*, 5374–5380.

56. Chou, T.C. (2010). Drug combination studies and their synergy quantification using the chou-talalay method. Cancer Res. *70*, 440–446.

57. Wang, D., Wang, Z., Tian, B., Li, X., Li, S., and Tian, Y. (2008). Two hour exposure to sodium butyrate sensitizes bladder cancer to anticancer drugs. Int. J. Urol. *15*, 435–441.

58. Rajaraman, S., Canjuga, D., Ghosh, M., Codrea, M.C., Sieger, R., Wedekink, F., Tatagiba, M., Koch, M., Lauer, U.M., Nahnsen, S., et al. (2019). Measles virus-based treatments trigger a pro-inflammatory cascade and a distinctive immunopeptidome in glioblastoma. Mol. Ther. Oncolytics *12*, 147–161.

59. Finck, R., Simonds, E.F., Jager, A., Krishnaswamy, S., Sachs, K., Fantl, W., Pe'er, D., Nolan, G.P., and Bendall, S.C. (2013). Normalization of mass cytometry data with bead standards. Cytometry. A. *83*, 483–494.

60. Chevrier, S., Crowell, H.L., Zanotelli, V.R.T., Engler, S., Robinson, M.D., and Bodenmiller, B. (2018). Compensation of signal spillover in suspension and imaging mass cytometry. Cell Syst. *6*, 612–620.e5.

61. Zunder, E.R., Finck, R., Behbehani, G.K., Amir, E.A.D., Krishnaswamy, S., Gonzalez, V.D., Lorang, C.G., Bjornson, Z., Spitzer, M.H., Bodenmiller, B., et al. (2015). Palladium-based mass tag cell barcoding with a doublet-filtering scheme and single-cell deconvolution algorithm. Nat. Protoc. *10*, 316–333.

62. Belkina, A.C., Ciccolella, C.O., Anno, R., Halpert, R., Spidlen, J., and Snyder-Cappione, J.E. (2019). Automated optimized parameters for T-distributed stochastic neighbor embedding improve visualization and analysis of large datasets. Nat. Commun. *10*, 5415–5512.